Target Localization with a Single Sensor via Multipath Exploitation

PAWAN SETLUR
GRAEME E. SMITH, Senior Member, IEEE
FAUZIA AHMAD, Senior Member, IEEE
MOENESS G. AMIN, Fellow, IEEE
Villanova University

In urban sensing and through-the-wall (TTW) radar, the existence of targets inside buildings results in multipath returns. These multipath returns are exploited to achieve target localization with a single sensor. A time-of-arrival (TOA) wall association algorithm is derived to relate multipath returns to their respective walls and targets, followed by a nonlinear least squares (NLS) optimization to localize the targets. Simulations and experimental data are used to validate the proposed algorithms.

Manuscript received December 7, 2010; revised April 4, 2011; released for publication June 2, 2011.

IEEE Log No. T-AES/48/3/943998.

Refereeing of this contribution was handled by F. Gini.

This work was sponsored by the U.S. Army Research Lab under Contract W911NF-07-D-0001.

Authors' address: Radar Imaging Lab, Center for Advanced Communications, Villanova University, 800 Lancaster Ave., Villanova, PA 19085, E-mail: (fauzia.ahmad@villanova.edu).

I. INTRODUCTION

The existence of targets in enclosed structures comprising walls, floors and ceilings, as in the case of through-the-wall (TTW) sensing, introduces multipath returns in the received radar signal. These returns could be confused for false targets, causing high false alarms in the conventional TTW localization system comprising an array of sensor elements. However, multipath can be exploited for target localization without the need to employ a physical or synthesized aperture. Instead, a single antenna radar system may be used. In essence, multipath returns may be utilized to provide additional virtual sensors permitting noncoherent target localization and such an approach is pursued in this paper. The single-sensor approach to urban target localization is a viable, cost effective, and physically smaller, sensing solution for target localization in TTW radar as well as in urban canyon situations [1–20].

TTW localization via a synthetic aperture radar (SAR) based system comprising multiple sensors has been extensively reported in the literature [5–12]. In [14] multipath was exploited, in the context of time reversal, to improve the beamformed image for a TTW scenario, but not for enlarged aperture. Noncoherent localization using multiple sensors for a single target in a TTW environment was analyzed in [12], [13], and references therein, but multipath was not specifically analyzed or exploited for target localization. Multipath exploitation techniques have also been reported in the literature [15–19, 21]. In [15] a range Doppler map for a single target direct line-of-sight (LOS) path and its multipath in an urban canyon is provided; the authors used both the single bounce as well as the double bounce multipath and a model for the multipath was assumed. In [16] a statistical detection technique was advocated for a single moving target in an urban canyon exploiting the specular multipath, and an orthogonal frequency division multiplexing (OFDM) radar model was proposed for incorporating the multipath Doppler shifts. The authors in [17] evaluated the potential for utilizing specular multipath reflections to improve detection for an airborne system. In [18] it was demonstrated experimentally that indoor targets, such as rotating fans and a walking person with a metal reflector, are detected via their respective multipath only. In [19] target tracking via multipath exploitation and waveform selection was developed assuming a 3D model in an urban canyon. A state space formulation was derived and a particle filter was used to track the target. The model assumed either constant Doppler or turning motions for a single target. In [21] multipath reflections were fused with the direct paths to achieve localization for pure reflectors using a passive sensing system with multiple sensors.

Our single-sensor-based technique exploits multipath to provide additional virtual sensors for localization and is quite different from the methods discussed above. Localization was neither the objective nor was it discussed in [15]–[18], whereas in [19], the authors fuse both the Doppler and the range information of a single target in a model to perform tracking. Our method, on the other hand, does not include any Doppler information, nor is it model specific. Unlike the multi-sensor approach taken in [21], we assume an active sensing system, which utilizes a single sensor for localization. In order to achieve single-sensor-based target localization, our approach assumes knowledge of the layout of surrounding walls and reflecting surfaces. This assumption is also made in [21] for fusing the multipath reflections into their weighted least squares cost function. The knowledge of surrounding walls may be available either through city and building blueprints or from prior surveillance operations [15–17, 19]. While surrounding walls in TTW sensing consist of side, front, and back walls, only two adjacent side walls are typically considered in urban canyon situations. We focus on the localization of targets using a single sensor by exploiting multipath returns. As part of the preprocessing required for our technique, it is necessary to suppress the dominant nontarget returns from the signal. For slow moving targets, this may be achieved through basic moving target indication (MTI) processing, such as pulse delay line cancellation [5]. While for stationary targets, the suppression may be achieved by the subtraction of a prerecorded reference scene from the data being processed.

In this paper, we cast target-wall multipaths as emanating from virtual sensors. We initially demonstrate the principle of target localization for a single target scene by utilizing the specular reflections from a single wall. It is then shown that, in the presence of additional walls, correct associations of the multipath returns with their respective walls must be performed. To this end, we derive an algorithm to trace each multipath's time-of-arrival (TOA) to its particular wall, and validate this association through simulation. For multiple targets, localization is achieved by sequentially grouping the TOAs for each target. The wall association routine is then applied to each group separately.

We primarily discuss target localization for the case of unobstructed LOS, i.e., in free-space. Since a front wall in TTW scenario encloses the target inside a rectangular room and separates it from the sensor, we also derive a nonlinear least squares (NLS) approach, which compensates for the wall propagation effects for accurate TTW target localization. The analysis presented here considers two-dimensional scenes with point targets, since this is sufficient to describe the technique. However, extensions to the third dimension, accounting for multipath reflections from the floor and ceiling, and to incorporate extended targets are a straightforward matter. The proposed techniques can be readily extended following the methodology in [9], [20].

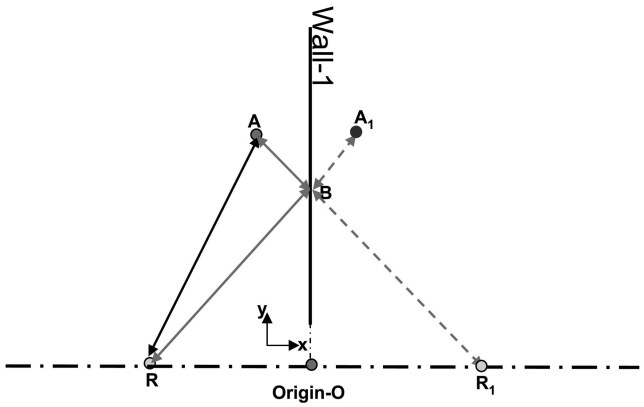

Fig. 1. Simple multipath model from single wall.

The remainder of the paper is organized as follows. In Section II the principle of localization via multipath is examined analytically, and a model incorporating the surrounding walls, namely two side walls and a back wall, is derived. We present an algorithm which allows the respective multipath TOAs to be associated correctly to their respective walls. In Section III multiple targets are considered and a TOA clustering technique is derived through which target localizations are achieved. In Section IV the devised techniques are tailored to address TTW target localization. Simulation and experimental results are provided in Section V, and conclusions are presented in Section VI.

II. MOTIVATION & MODEL

A. Motivation

Consider Fig. 1 which shows the sensor-target geometry. There is a single sensor (monostatic radar) at point R and a target at point A, which is adjacent to a smooth reflecting wall (wall 1). The position vectors of the radar and the target are, respectively, given by $\mathbf{R} = [-D_x, 0]^T$ and $\mathbf{x}_t = [-x_t, y_t]^T$ in the Cartesian coordinate system. We assume that the radar waveform is sufficiently wideband so that the multipath and direct path returns are resolved.

The direct path return corresponds to the signal that propagates to and from the target along the direct path RA. In addition to the direct path, there is an indirect path RBA by which the signal may reach the target. This indirect path involves a reflection on the wall at point B. There are two types of multipath returns, which arise because of the different permutations of the round trip the signal may take to the target when path RBA is considered. The first type corresponds to the first-order multipath, in which the signal round trip consists of a leg along path RA,

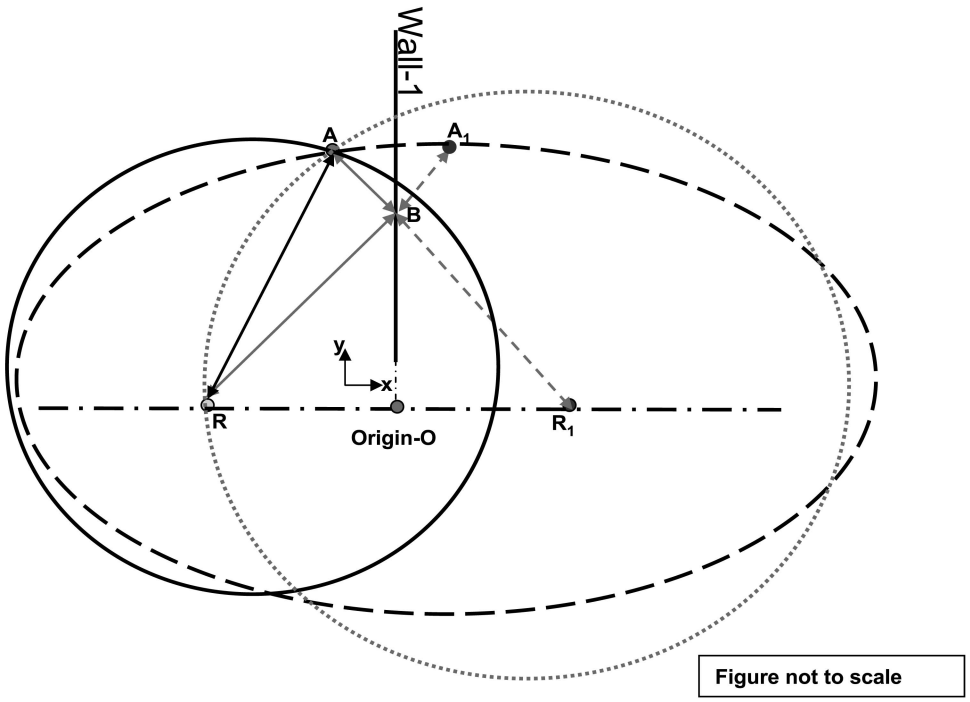

Fig. 2. Principle of localization.

and a leg along path *RBA*. The order in which the signal propagates along the two paths is not important. Traveling out along *RA* and returning along *RBA* has the same TOA as traveling out along *RBA* and returning along *RA*; both permutations, therefore, lead to a single return. The second type is the second-order multipath, which travels to and from the target along path *RBA*. Depending on the context, both the first- and second-order multipath returns are referred to generally as multipath in the rest of the paper.

The smoothness assumption of wall 1 implies specular reflections at point B. As a result we observe from Fig. 1 that reflecting the indirect path about wall 1 yields an alternative radar-target geometry. The point R_1 is defined as the virtual radar and $R_1B = RB$. Additionally, we obtain the virtual target denoted as A_1 and $A_1B = AB$. It is readily seen from the geometry that the virtual target and the virtual radar position vectors are given by $[x_t, y_t]^T$ and $[D_x, 0]^T$, respectively. Considering Fig. 2, we observe that the first-order multipath has the same time delay as a bistatic configuration, comprising the radar and the virtual radar. That is, in terms of the range, we have

$$RA + AB + BR = RA + RA_1 = RA + R_1A \tag{1}$$

where $RA + R_1A$ represents the bistatic configuration, i.e., the signal propagates from the radar to the target, and is received by the virtual radar. The constant range contour corresponding to the first-order multipath, represented by the dashed line in the figure, is thus an ellipse, which has foci at the radar and the virtual radar and passes through the target and the virtual target locations. On the other hand, the round trip along the direct path and the second-order multipath, being monostatic measurements, have circular constant range contours (the solid black and dotted gray lines), centered, respectively, at the radar and the virtual radar, with both passing through the target location. Both the circles and the ellipse, therefore, intersect at the true target location $\mathbf{x}_t$. Mathematically, we seek a common intersection point of

$$\begin{aligned}
&\frac{x^2}{a_1^2} + \frac{y^2}{a_1^2 - c_1^2} = 1 \\
&a_1 := \frac{\sqrt{(x_t + D_x)^2 + y_t^2} + \sqrt{(x_t - D_x)^2 + y_t^2}}{2} \\
&c_1 := D_x \\
&(x + D_x)^2 + y^2 = (x_t - D_x)^2 + y_t^2 \\
&(x - D_x)^2 + y^2 = (x_t + D_x)^2 + y_t^2
\end{aligned} \tag{2}$$

where the first expression is the equation for the ellipse, and the remaining two expressions in (2) are the equations for the circles. There exist two solutions to this system of equations; the first is the true target location $\mathbf{x}_t$, and the other is at $[-x_t, -y_t]^T$, which is behind the radar.

B. Free-Space Model

In practice when considering multiple walls such as those shown in Fig. 3, additional processing must be performed, which is not applicable in the single-wall scenario. In essence, the TOAs will need to be associated to the sources of multipath,

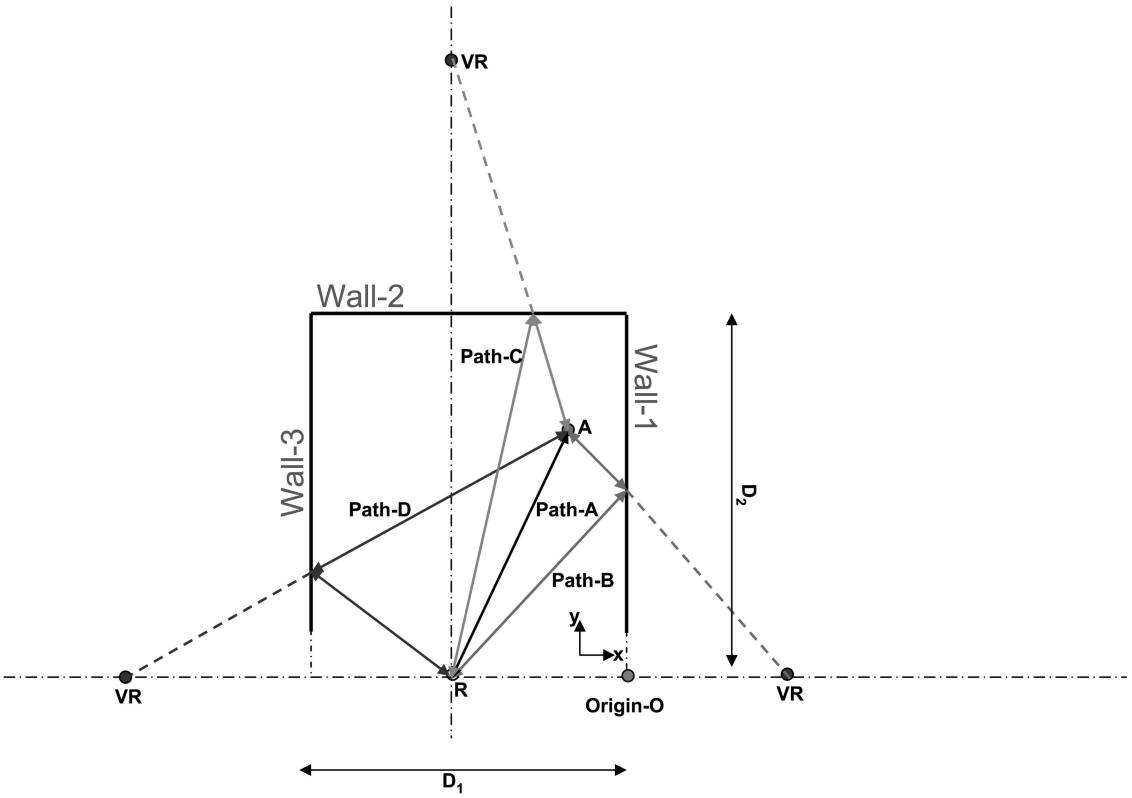

Fig. 3. Free-space model and scene.

namely walls 1, 2, and 3. Without correct associations, the ellipses and circles may not all intersect at the true target coordinates. Figure 3 represents an urban canyon type geometry in which the target is located at $\mathbf{x}_t$. Specular multipath is considered. The location and the extent D_i, $i = 1,2$, of the side and back walls are assumed known. The rest of the target and radar parameters are identical to those in Figs. 1 and 2. For clarity, the direct path is denoted as path A, whereas the multipath from walls 1, 2, 3 is, respectively, denoted as paths B, C, and D. Higher order multipaths, which incorporate multiple reflections at the walls, are ignored as they suffer from severe fading and may be too weak to be observed [19]. Nonetheless, such higher order paths, if sufficiently pronounced, can be incorporated in a straightforward manner as demonstrated in [20].

The radar transmits a pulsed waveform $s(t)$, where "t" indexes the time within the pulse, and measures the received signal. The received signal is a superposition of the direct path and the multipath returns, given by

$$z(t) = \sum_{p\in\{A,B,C,D\}} \Gamma_p^2 s(t-\tau_p) + 2\sum_{q\in\{B,C,D\}} \Gamma_A\Gamma_q s(t-(\tau_p+\tau_q)/2) + n(t) \quad (3)$$

where τ_p and Γ_p are, respectively, the TOA and the complex amplitude associated with reflection and transmission coefficients for one-way propagation along path p, and $n(t)$ is the system noise. The amplitude Γ_p can be readily derived, provided the material properties of the walls are known [20, 22]. Without loss of generality, we assume that $\Gamma_p = 1$, $\forall p$, $p \in \{A,B,C,D\}$. From the geometry, it is clear that (3) includes a total of seven signal returns, and the TOA of each return can found by a conventional matched filtering process followed by peak detection. In the event of the TOAs being close together, or the signal-to-noise ratio (SNR) being poor, alternative techniques, such as the super resolution MUSIC or the inverse correlation method, may be used [23, 24]. For the remainder of the algorithm description, we assume the TOAs are accurately detected. By virtue of propagation and reflections, the TOAs are naturally ordered in an ascending fashion, which may be represented in vector form as

$$\boldsymbol{\tau} = [\tau_1,\tau_2,\ldots,\tau_7]^T, \quad \tau_1 = \tau_A, \quad \tau_i < \tau_{i+1}, \quad i = 1,2\ldots,7. \quad (4)$$

In (4) the first TOA always corresponds to the direct path. The rest of the TOAs are unascertained. For example, it is not known if τ_4 is a first-order or a second-order multipath TOA, nor which particular wall is responsible for it. Therefore, two fundamental problems arise in multipath analyses; first, determining which TOAs are first order and

which are second order, and how to pair the multipath returns that originate from the same wall; and second, determining which wall caused a particular pair of TOAs.

First, the problem of pairing the multipath returns is considered. Initially, we observe that the first TOA in $\boldsymbol{\tau}$, $\tau_1 = \tau_A$, is known to be the direct path and that the last TOA, τ_7, must be a second-order multipath. Next we note that if τ_p, when $2 \le p < 7$, is considered to be a first-order multipath, only those τ_q, where $p < q \le 7$, could be the second-order multipath TOA caused by the same wall. Using the knowledge that TOA of a first-order multipath is one half of the sum of the TOAs of the direct path and the matching second-order multipath, e.g., for wall 1 in Fig. 3, $\tau_{AB} = (\tau_A + \tau_B)/2$, a cost function may be developed for the possible valid pairings of first- and second-order multipath. If a TOA τ_p, where $2 \le p < 7$, is a candidate for being a first-order multipath, then for a second-order multipath candidate τ_q, where $p < q \le 7$, from the same wall, we may write

$$|(\tau_1 + \tau_q)/2 - \tau_p| = \begin{cases} 0 & \text{if } \tau_q \text{ is the second order to } \tau_p \\ a & \text{where } a > 0, \text{ if } \tau_q \text{ is not the second order to } \tau_p \end{cases} \tag{4a}$$

assuming there is no error in the TOA measurements. By considering all valid pairs of τ_p and τ_q for $p = 2,\ldots,7$, an ordered cost vector can be formed as

$$\begin{aligned} \boldsymbol{\tau}_{\cos t} = \text{sort}\{[&|\tau_A/2 + \tau_3/2 - \tau_2|, |\tau_A/2 + \tau_4/2 - \tau_2|, \ldots, \\ &|\tau_A/2 + \tau_7/2 - \tau_2|, \ldots, \\ &|\tau_A/2 + \tau_6/2 - \tau_7|]^T\} \end{aligned} \tag{5}$$

where the operator sort$\{\cdot\}$ arranges the elements in increasing order. The vector in (5) is comprises 15 elements when three walls are considered. For three walls, the first three elements in (5) indicate the correct pairing of the first- and second-order multipath returns. From the first three elements of $\boldsymbol{\tau}_{cost}$, we can extract "pair vectors," $\boldsymbol{\tau}^{(k)}$, $k = 1,2,3$, to store the associated multipath return TOAs. The structure of each $\boldsymbol{\tau}^{(k)}$ will be a two-element vector defined as $\boldsymbol{\tau}^{(k)} = [\tau_q^{(k)}, \tau_p^{(k)}]^T$, where $\tau_p^{(k)}$ and $\tau_q^{(k)}$ are the multipath TOAs from the kth element of $\boldsymbol{\tau}_{cost}$. Before moving on, it is important to realize that the index k of $\boldsymbol{\tau}^{(k)}$ does not indicate which wall the TOAs are associated with.

Second, the problem of wall association is addressed. Ideally, when the TOAs are correctly associated, we have, for wall 1, the bistatic ellipse, corresponding to the first-order multipath return, and monostatic circular contour centered at the virtual radar, corresponding to the second-order multipath. These can be arranged in a vector format as

$$\begin{aligned} \beta_1(\tau_{AB}) &= \frac{4x^2}{\tau_{AB}^2 c^2} + \frac{4y^2}{(\tau_{AB}^2 c^2 - 4D_x^2)} - 1 = 0 \\ \beta_2(\tau_B) &= (x - D_x)^2 + y^2 - \tau_B^2 c^2/4 = 0 \\ \boldsymbol{\beta}_{\mathbf{w_1}} &:= [\beta_1(\tau_{AB}), \beta_2(\tau_B)]^T \end{aligned} \tag{6}$$

where c is the speed of light in free space. Similarly, for wall 2 we have

$$\begin{aligned} \beta_3(\tau_{AC}) &= \frac{4(x + D_x)^2}{(\tau_{AC}^2 c^2 - 4D_2^2)} + \frac{4(y - D_2)^2}{\tau_{AC}^2 c^2} - 1 = 0 \\ \beta_4(\tau_B) &= (x + D_2)^2 + (y + 2D_2)^2 - \tau_C^2 c^2/4 = 0 \\ \boldsymbol{\beta}_{\mathbf{w_2}} &:= [\beta_3(\tau_{AC}), \beta_4(\tau_C)]^T. \end{aligned} \tag{7}$$

Likewise, for wall 3,

$$\begin{aligned} \beta_5(\tau_{AD}) &= \frac{4(x - D_1 + D_x)^2}{\tau_{AD}^2 c^2} + \frac{4y^2}{(\tau_{AD}^2 c^2 + 4D_x^2 - 4D_1^2)} - 1 \\ &= 0 \\ \beta_6(\tau_D) &= (x + 2D_1 - D_x)^2 + y^2 - \tau_D^2 c^2/4 = 0 \\ \boldsymbol{\beta}_{\mathbf{w_3}} &:= [\beta_5(\tau_{AD}), \beta_6(\tau_D)]^T. \end{aligned} \tag{8}$$

Lastly, for the monostatic direct path, we have the circular constant range contour,

$$\beta_7(\tau_A) = (x + D_x)^2 + y^2 - \tau_A^2 c^2/4 = 0. \tag{9}$$

The expressions defined in (6)–(9) can be concatenated into a single vector $\boldsymbol{\beta}$ defined as

$$\boldsymbol{\beta} := [\boldsymbol{\beta}_{\mathbf{w_1}}^T, \boldsymbol{\beta}_{\mathbf{w_2}}^T, \boldsymbol{\beta}_{\mathbf{w_3}}^T, \beta_7(\tau_A)]^T.$$

This vector is a function of the coordinates x and y, combined into a vector $\mathbf{x}$, the three pairs of first- and second-order multipath TOAs $\boldsymbol{\tau}^{(k)}$, $k = 1,2,3$, and the direct path TOA τ_A. In full, the vector-function would be written as $\boldsymbol{\beta}(\mathbf{x}, [\boldsymbol{\tau}^{(1)T}, \boldsymbol{\tau}^{(2)T}, \boldsymbol{\tau}^{(3)T}], \tau_A)$ but this full description has been omitted above for clarity. Clearly, when the wall associations are correct and the TOAs estimates are perfect,[1] the circles and ellipses in (6)–(9) all intersect at one location and,

$$\|\boldsymbol{\beta}\|^2 = 0. \tag{10}$$

However, for imperfect TOA measurements, we seek the vector $\mathbf{x}$ and the set of pairs of first- and second-order multipath TOAs that will minimize $\|\boldsymbol{\beta}\|^2$.

The possible sets of pairs of first- and second-order multipath TOAs are limited. Consider the matrix, comprising all permutations of $\boldsymbol{\tau}^{(k)T}$,

[1] Measured TOAs after matched filtering are quantized to belong to range gates, and adjacent range gates are separated by the system range resolution. Hence, in practice, the ellipses and circles do not all intersect at one common point but approximately intersect in a region.

$k = 1,2,3,$

$$\mathbf{E}_{perm} := \begin{array}{c} \text{wall 1} \quad \text{wall 2} \quad \text{wall 3} \\ \begin{bmatrix} \boldsymbol{\tau}^{(1)T} & \boldsymbol{\tau}^{(2)T} & \boldsymbol{\tau}^{(3)T} \\ \boldsymbol{\tau}^{(1)T} & \boldsymbol{\tau}^{(3)T} & \boldsymbol{\tau}^{(2)T} \\ \vdots & \vdots & \vdots \\ \boldsymbol{\tau}^{(3)T} & \boldsymbol{\tau}^{(1)T} & \boldsymbol{\tau}^{(2)T} \end{bmatrix} \end{array} := \begin{bmatrix} \mathbf{e}_1 \\ \mathbf{e}_2 \\ \vdots \\ \mathbf{e}_6 \end{bmatrix} \in \Re^{3!\times 3!}. \tag{11}$$

In (11) for example, the second row third column implies that $\boldsymbol{\tau}^{(2)}$ was assigned to wall 3. Likewise, similar implications may be seen from (11). The elements of the row vectors $\mathbf{e}_j$ now contain the possible sets of pairs of first- and second-order multipath TOAs. In the spirit of (10), the NLS error is minimum for the correct permutation in (11), i.e.,

$$\hat{\mathbf{x}}_t = \min_{\mathbf{x}:=[x,y]^T, j} \{\|\boldsymbol{\beta}(\mathbf{x}, \mathbf{e}_j, \tau_A)\|^2\}, \qquad j = 1,2\ldots,6 \tag{12}$$

where the minimum is taken over all j. Equations (10) and (12) can be solved using numerical optimization. We implemented this minimization using the "lsqnonlin" function in the Matlab Optimization Toolbox, initialized with coordinates of the center of the room. Note that the function to be minimized in (12) is overdetermined consisting of two unknowns and seven equations. Hence, target localization could still be achieved using the multipath returns alone even if the direct path was completely ignored.

III. MULTIPLE TARGETS

Increasing the number of targets in the scene also increases the number of TOAs that need pairing and associating to walls. Fortunately, an approach similar to the single-target case for identifying the first- and second-order multipath and associating the pairs to the walls can be applied. Consider K targets. As in (4), the TOAs stored in the vector $\boldsymbol{\tau}$ have a naturally increasing order, but now there are $7K$ elements, i.e.,

$$\boldsymbol{\tau} = [\tau_1, \tau_2, \ldots, \tau_{7K}]^T, \qquad \tau_i < \tau_{i+1}, \quad i = 1,2\ldots,7K. \tag{13}$$

The first TOA τ_1 corresponds to the direct path return of the target closest in range to the radar. The rest of the TOAs are unascertained. Our approach is to first cluster the TOAs corresponding to the nearest target, and identify its first- and second-order multipath TOAs, and their association with the walls. This procedure is then continued for the second nearest target, then the third, and so on until all K targets have been exhausted. This sequential process is depicted below.

1) *Initialize*: Let target count $K_1 = 0$ and set a temporary time delay vector, $\hat{\boldsymbol{\tau}} = \boldsymbol{\tau}$.

2) *Loop*: Repeat until $K_1 = K$. For index $k = 2,\ldots,7(K - K_1)$ calculate and store the minimum cost of the set

$$\{\tau_{cost}^k\} = \min\{(\tau_1/2 + \tau_{k_1}/2 - \tau_k)\}, \quad k_1 \neq k, \quad k_1 \in \{2,3,\ldots,7(K-K_1)\}. \tag{14}$$

3) *Search*: Find and store the TOAs corresponding to the k_1-indices of the first three minima in the set $\{\tau_{cost}^k\}$, as well as the TOAs associated with indices (ks). The k_1 indices represent the second-order multipaths, and the ks are locations of the associated first-order multipaths in $\hat{\boldsymbol{\tau}}$.

4) *Store*: Save the first TOA in $\hat{\boldsymbol{\tau}}$, and the TOAs corresponding to the k_1-indices of the first three minima in the set $\{\tau_{cost}^k\}$, and the corresponding TOAs indexed by the three ks of step 3 in a vector denoted by $\hat{\boldsymbol{\tau}}_{K_1}$.

5) *Associate and Localize*: Using the wall association procedure as described in Section II, compute the coordinates for the K_1th target.

6) *Modify*: Increment target counter as $K_1 = K_1 + 1$, since we have clustered the direct and multipath TOAs corresponding to the K_1th target in $\hat{\boldsymbol{\tau}}_{K_1}$. Using a set difference operator, $\{-\}$, remove the elements in $\hat{\boldsymbol{\tau}}_{K_1}$ from $\hat{\boldsymbol{\tau}}$ by

$$\hat{\boldsymbol{\tau}} = \hat{\boldsymbol{\tau}}\{-\}\hat{\boldsymbol{\tau}}_{K_1}. \tag{15}$$

7) *Check*: Sort the elements in ascending order in the new vector, $\hat{\boldsymbol{\tau}}$. Go back to step 2.

It is noted that in step 2 of the algorithm and especially in (14), we considered only the minimum cost for every k. The algorithm performs as desired when all the direct paths and all the multipaths corresponding to the K targets are resolved and detected. However, the algorithm as described above has two shortcomings. First, when target-target or target-clutter interactions create spurious peaks in the range profile with TOAs that satisfy the rule in (4a) when combined with other genuine TOAs, the algorithm will fail to localize the targets. Second, a reduced number of TOAs will be detected if 1) two or more of the direct paths and first- or second-order multipaths are the same length, resulting in unresolved peaks in the range profile, and 2) some of the direct paths and multipaths fall below the noise and fail detection. While the minimization of (12) is overdetermined, and thus can still find the target location with unresolved/undetected TOAs, the wall association and target clustering algorithms are not robust to this situation. In essence, while the presented algorithm would fail if some peaks in the range profile are unresolved or undetected, this failure is a result of the simple association and clustering schemes presented here and not the underlying concept of single-sensor target localization achieved through the minimization in (12). We further note that when the

targets of interest are moving, it is unlikely that the range profiles will contain spurious/unresolved peaks all of the time. Occasional failure of the routine to provide an update could then be overcome by using a robust tracker, which is beyond the scope of this work.

Rather than relying on a tracker, the robustness of the association and clustering routines can be improved at the expense of computational complexity. Consider a scene comprising two targets and assume that the number of detected TOAs is 16, which is two more than the 14 TOAs expected from two genuine targets. We may choose a combinatorial approach to resolve this issue. That is, we select, say, the first 14 TOAs from the set of 16 detected TOAs, and use the algorithm described above in steps 1–7 to provide target location estimates and record the corresponding NLS cost. We then choose another set of 14 TOAs from the 16 detected TOAs, and obtain the corresponding location estimates and associated NLS cost. We repeat this process for all ${}^{16}\mathbb{C}_{14} = 16!/14! \times 2! = 120$ combinations of choosing 14 TOAs from the 16 detected TOAs. Finally, the recorded NLS costs for all 120 combinations are compared and the target location estimates corresponding to the combination which yields the minimum NLS cost are chosen as the solution to the target localization problem. In general, for N detected TOAs with K targets ($N > K$), the number of combinations to be evaluated is ${}^{N}\mathbb{C}_{K}$. The inherent problem with this approach is that a small increase in the number of targets or the number of detected TOAs results in an exponential increase in the total number of combinations. However, we note that for the case of undetected TOA, the combinatorial approach may cause some of the targets to be either wrongly localized or completely missed. Simulation examples involving the combinatorial solution are relegated to Section V.

IV. THROUGH-THE-WALL OPERATION

When operating through the wall, the free-space approach taken above is unsuitable. The localization technique outlined in Section II depends on the knowledge of the shape of the constant range contours. Even when the wall parameters are known, the constant range contours for a given TOA under TTW operation would not have closed-form expressions. This prevents formulation of an NLS approach in a manner outlined above. Fortunately, as we demonstrate in this section, an alternative NLS solution is possible that allows for incorporation of the effects of the wall. However, the TTW solution requires an iterative root finding operation to solve for angles of refraction associated with TTW propagation [20] for every candidate target location, which significantly increases the computational burden, and makes it sensitive to initial conditions. To circumvent these difficulties, good quality initial estimates of the target locations are required. These estimates can be obtained by treating the TTW measurements as if it were free-space propagation and using the free-space algorithm described in Section III. The free-space target location estimates have been demonstrated to provide reasonable initialization for iterative techniques [12].

For TTW operation, the signal returns are non-LOS and the propagation inside the wall must be taken into account for accurate localization. Consider Fig. 4 which shows the model for a target in an enclosed structure. There is a front wall and walls 1, 2, 3. The front wall has known thickness and dielectric constant given by d_1 and ε_1, respectively. Similar to the free-space case, we consider the direct path, referred to as path A, and three additional paths, namely, paths B, C, and D, which correspond to the multipaths. Note, however, that the TOAs are not identical to the free-space propagation and now depend on the slowing of the wave within the front wall and the reflection and refraction that occurs at the wall boundaries [9, 12, 20].

For target localization, an NLS procedure can be initialized with the free-space solutions. Consider the vector $\boldsymbol{\tau}_k$, $k = 1,2\ldots,K$, which consists of the TOAs corresponding to the direct path, and the first- and second-order multipath returns for the kth target. Specifically,

$$\begin{aligned} \boldsymbol{\tau}_k &= [\tau_{1k}, \tau_{2k}, \ldots, \tau_{7k}]^T, \\ \tau_{1k} &= \tau_{Ak}, \qquad \tau_{5k} = \frac{\tau_{Ak} + \tau_{2k}}{2}, \\ \tau_{6k} &= \frac{\tau_{Ak} + \tau_{3k}}{2}, \qquad \tau_{7k} = \frac{\tau_{Ak} + \tau_{4k}}{2}. \end{aligned} \tag{16}$$

The vector $\boldsymbol{\tau}_k$ is obtained by the clustering algorithm outlined in Section III. In (16) the first time delay corresponds to the direct path of the kth target, and is denoted likewise. The TOAs τ_{2k}, τ_{3k}, and τ_{4k} correspond to the second-order multipath, whereas the remaining TOAs in (16) are their first-order multipaths. For multipath-wall association, we resort to (12) and apply NLS solutions for each target k. Initialization is performed by solving a similar free-space equation separately for each one of the six possible associations (permutations), i.e.,

$$\mathbf{x}_{kj}^{\mathrm{FS}} := \min_{\mathbf{x}} \{\beta(\mathbf{x}, \mathbf{e}_{kj}, \tau_{k1})\}, \qquad j = 1,\ldots,6 \tag{17}$$

where $\mathbf{e}_{kj}$, $j = 1,\ldots,6$, is the permutation vector for the kth target. The difference between (11) and (17) is that in the former, minimization is performed over all j, whereas in the latter, minimization is performed for a particular j. In other words, (11) gives a single free-space solution, whereas (17)

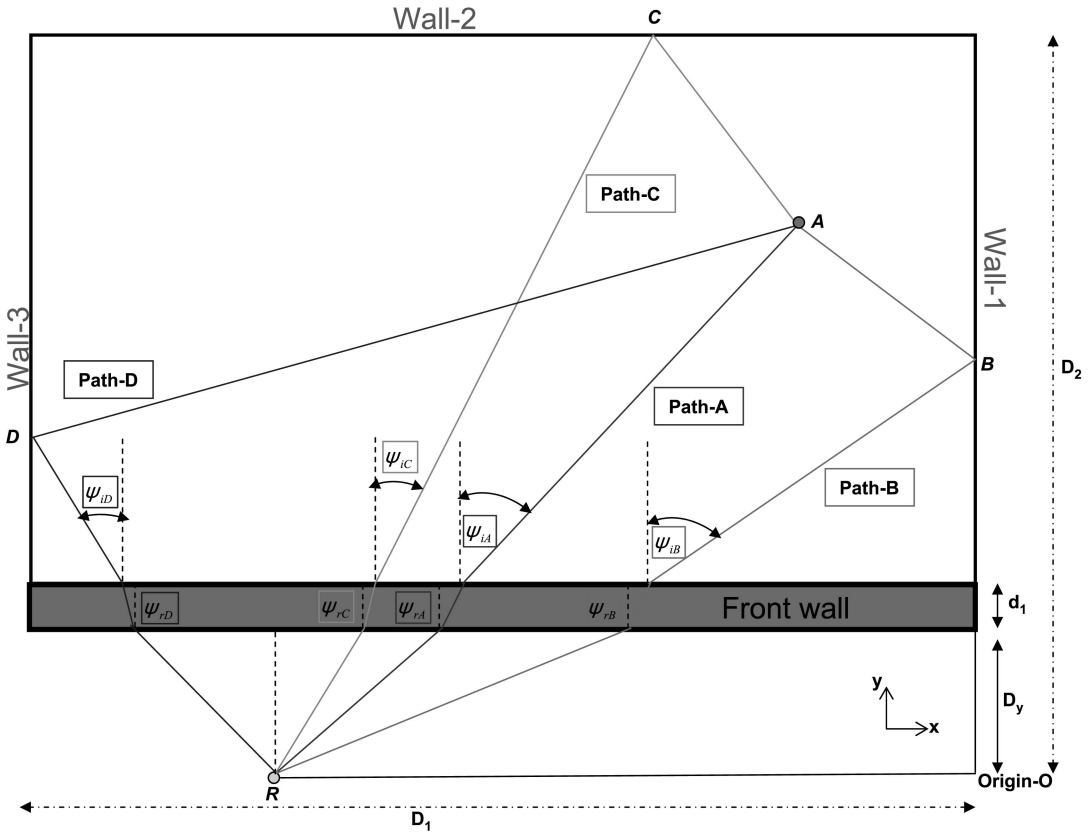

Fig. 4. TTW model for single target.

provides six free-space solutions of the target position. The proposed algorithm is described below.

1) *Cluster*: Cluster the kth TTW target's direct path, first- and second-order multipath TOAs and store them in a vector $\boldsymbol{\tau}_k$. The clustering is performed using the algorithm for multiple targets, and also identifies whether particular TOA is either a first-order or second-order multipath.

2) *Compute*: Assuming a free-space model, compute the various free-space solutions $\mathbf{x}_{kj}^{\mathrm{FS}}$ as in (17) for all possible wall permutations. These free-space solutions are used to initialize the actual TTW NLS localization estimator.

3) *NLS*: For a particular j, consider the optimization, initialized with the free-space solution, $\mathbf{x}_{kj}^{\mathrm{FS}}$

$$\begin{aligned}\mathbf{x}_k^{\mathrm{TTW}} &= \min_{\mathbf{x}',j} \|\mathbf{e}'_{kj} - \boldsymbol{\tau}'\|^2, \ \textit{initialized with}\ \mathbf{x}_{kj}^{\mathrm{FS}}, \\ &\qquad j = 1,2\ldots,6 \\ \mathbf{e}'_{kj} &:= [\tau_{1k}, \mathbf{e}_{kj}^T]^T, \quad \mathbf{x}' := [x', y']^T \\ \boldsymbol{\tau} &:= [\tau'_A(\psi'_{iA}), \tau'_B(\psi'_{iB}), \ldots, \tau'_D(\psi'_{iD}), \tau'_A(\psi'_{iA})/2 \\ &\quad + \tau'_B(\psi'_{iB})/2, \ldots, \tau'_A(\psi'_{iA})/2 + \tau'_D(\psi'_{iD})/2]^T\end{aligned} \tag{18}$$

with $\mathbf{x}_{kj}^{\mathrm{FS}}$, for which the vector $\boldsymbol{\tau}'$ can be found by computing the angles, ψ'^{s}_{ip}, $p \in \{A,B,C,D\}$. The angles can be computed by solving the equations numerically,

$$\begin{aligned} d_1 \tan(\psi'_{rA}) + (y' - d_1)\tan(\psi'_{iA}) - D_x + x' &= 0 \\ d_1 \tan(\psi'_{rB}) + (y'_B - d_1)\tan(\psi'_{iA}) - D_x &= 0 \\ (2D_2 - y')\tan(\psi'_{iC}) & \\ + d_1(\tan(\psi'_{rC}) - \tan(\psi'_{iC})) - D_x + x' &= 0 \\ d_1 \tan(\psi'_{rD}) + (y'_D - d_1)\tan(\psi'_{iD}) - D_1 + D_x &= 0 \\ \psi'_{rp} = \sin^{-1}\left(\frac{\sin(\psi'_{ip})}{\sqrt{\varepsilon_1}}\right), \qquad p &\in \{A,B,C,D\} \end{aligned} \tag{19}$$

where y'_B and y'_D can be substituted by

$$\begin{aligned} y'_B &= y' - x'\cot(\psi'_{iB}) \\ y'_D &= y' - (D_1 - x')\cot(\psi'_{iD}). \end{aligned} \tag{20}$$

Repeat the procedure $\forall j$. The TTW kth target location estimate $\mathbf{x}_k^{\mathrm{TTW}}$ is obtained as one which yields the minimum cost in (18) $\forall j$.

4) *Check*: Stop if all the k targets have been localized, otherwise go to step 1 and repeat.

In step 4, without invoking unnecessary mathematical operators, and for meaningful interpretation of the NLS cost, it is assumed that the elements in $\mathbf{e}'_{kj}$ are ordered in an identical fashion as in $\boldsymbol{\tau}'$. In other words, in line with the current permutation, the first element in $\mathbf{e}'_{kj}$ is the direct path, the next three elements are the second-order multipath

TOAs, corresponding to paths B, C, D, while the remaining elements are their associated first-order multipath TOAs. Furthermore, in (18) the elements of $\boldsymbol{\tau}'$ depend on the angles ψ'_{ip}, $p \in \{A,B,C,D\}$. These angles are highly nonlinear functions of $\mathbf{x}'$. The angles are obtained by solving the equations in (19) using (20). We note that obtaining the angles includes an inherent optimization, albeit in a single variable for each path. In essence, (18) consists of an explicit NLS stage, and an implicit root finding stage to obtain the angles [20], necessary to construct the TOAs in $\boldsymbol{\tau}'$. For the correct wall association, it is readily seen that the minimum is obtained.

In the above algorithm, the free-space solutions are essential to estimate the TTW target locations. It is noted that the above formulation involves wall association along with the NLS and the root finding to compute the precise through-wall angles. If one is confident that, for each of the k targets, the free-space wall associations are correct when applied to the TTW scenario, then (17) may be circumvented, and the free-space approach may be used directly to obtain the final free-space solution. That is, one can use (11)–(12) to obtain $\mathbf{x}_k^{\text{FS}}$. Our formulation for the TTW problem, however, is more general, and does not place complete confidence in the approach of using the free-space wall association for the TTW TOAs.

V. SIMULATIONS AND EXPERIMENTAL RESULTS

A. Free-Space: Single-Target Scenarios

The target locations and dimensions of the walls, etc., are all in meters unless noted otherwise. Consider a single target at $\mathbf{x}_t = [-16.7, 8.6]^T$ in the scene identical to Fig. 3. The parameters $D_1 = 20$ and $D_2 = 15$ and the radar's coordinates are given by $R = [-12, 0]^T$. Figure 5 shows the various constant range ellipses and circles with respect to the walls 1,2,3 for the considered scene. In particular, the six subfigures, namely, Fig. 5(a)–(f), show the intersection of the various ellipses and circles for all possible permutations of the first- and second-order multipath TOAs as given in (11). The TOAs (hence ranges) used in Fig. 5(a)–(f) are exact and are derived from simple geometry. In these figures, the true target location is indicated by "□", the actual radar and the virtual radar locations are all marked by "*", and the origin is indicated by "O". The walls are depicted as black dashed lines in the figures. The monostatic circular constant range contour centered at the actual radar, i.e., corresponding to the direct path TOA is always shown by a solid black line. By the convention adopted in the rest of this section, the virtual radars are in gray, and the actual radar is in black. Likewise, the elliptical bistatic constant range contours and the circular monostatic constant range contours centered at the virtual radars are plotted in gray and black, respectively. In particular for the ellipses, they are depicted as solid lines for wall 1, dashed lines for wall 2, and dashed-dotted lines for wall 3. Similarly the monostatic circles centered at the virtual radars are shown as dashed lines for wall 1, dotted lines for wall 2, and dashed-dotted lines for wall 3. The six different permutations (or wall associations) can be inferred from the figure titles. For example, consider Fig. 5(a)'s title, which states that the respective TOAs of wall 1 have been assigned correctly to wall 1, whereas TOAs arising from reflections at wall 2 are assigned to wall 3 while wall 3's TOAs are assigned to wall 2. The last permutation, shown in Fig. 5(f), corresponds to the correct wall associations. The NLS costs in (12) for each of the permutations in Fig. 5 are provided in the first row of Table I. From this table, it is evident that the NLS of (12) would choose the last permutation to be the correct wall association yielding the estimated target coordinates, $\hat{\mathbf{x}}_t = [-16.69, 8.6]^T$.

In several parts of Fig. 5, one of the bistatic ellipses has collapsed to a line between the sensor and the virtual sensor. The collapse arises when the solution to the ellipse equation is purely imaginary for one axis; in the figure, only the real part is plotted. In practice, the solutions to the ellipse and circle equations must be real. If complex solutions are obtained, then the related permutations can be discounted as invalid without presentation to the NLS optimizer. This yields a computational saving. We note, however, that NLS optimizer still achieves localization even if these invalid permutations are presented.

Figure 6 shows the results for the same scene as for Fig. 5, but with the target at position $\mathbf{x}_t = [-4.7, 7.6]^T$. The result for the correct wall association is presented in Fig. 6. The corresponding NLS costs for all 6 permutations are provided in the second row of Table I, where the cost of the correct solution is observed to be several orders of magnitude less than the other possibilities.

B. Free-Space: Multiple Targets with Noise

Next, consider two targets at coordinates $\mathbf{x}_t^{(1)} = [-15.4, 8]^T$ and $\mathbf{x}_t^{(2)} = [-4.6, 5.6]^T$ in a scene similar to Fig. 3 with an SNR of 15 dB assuming the noise is additive, white, and complex Gaussian. The radar transmits a rectangular pulse with bandwidth equal to 1.2 GHz, and carrier frequency set at 2 GHz. The rest of the parameters are identical to the single-target scenarios corresponding to Figs. 5 and 6. In Fig. 7(a), peaks of the range profile after matched filtering are shown. There are several peaks corresponding to the direct path and first- and second-order multipath returns for the two targets. It is noted that some of the peaks, although resolvable, are close to each other. Application of the processing from Section III leads to Fig. 7(b), which confirms that both targets have been localized correctly. The NLS estimates for the locations are given by $\hat{\mathbf{x}}_t^{(1)} = [-15.398, 8.007]^T$ and $\hat{\mathbf{x}}_t^{(2)} = [-4.58, 5.679]^T$. The errors in these solutions are in the second decimal place.

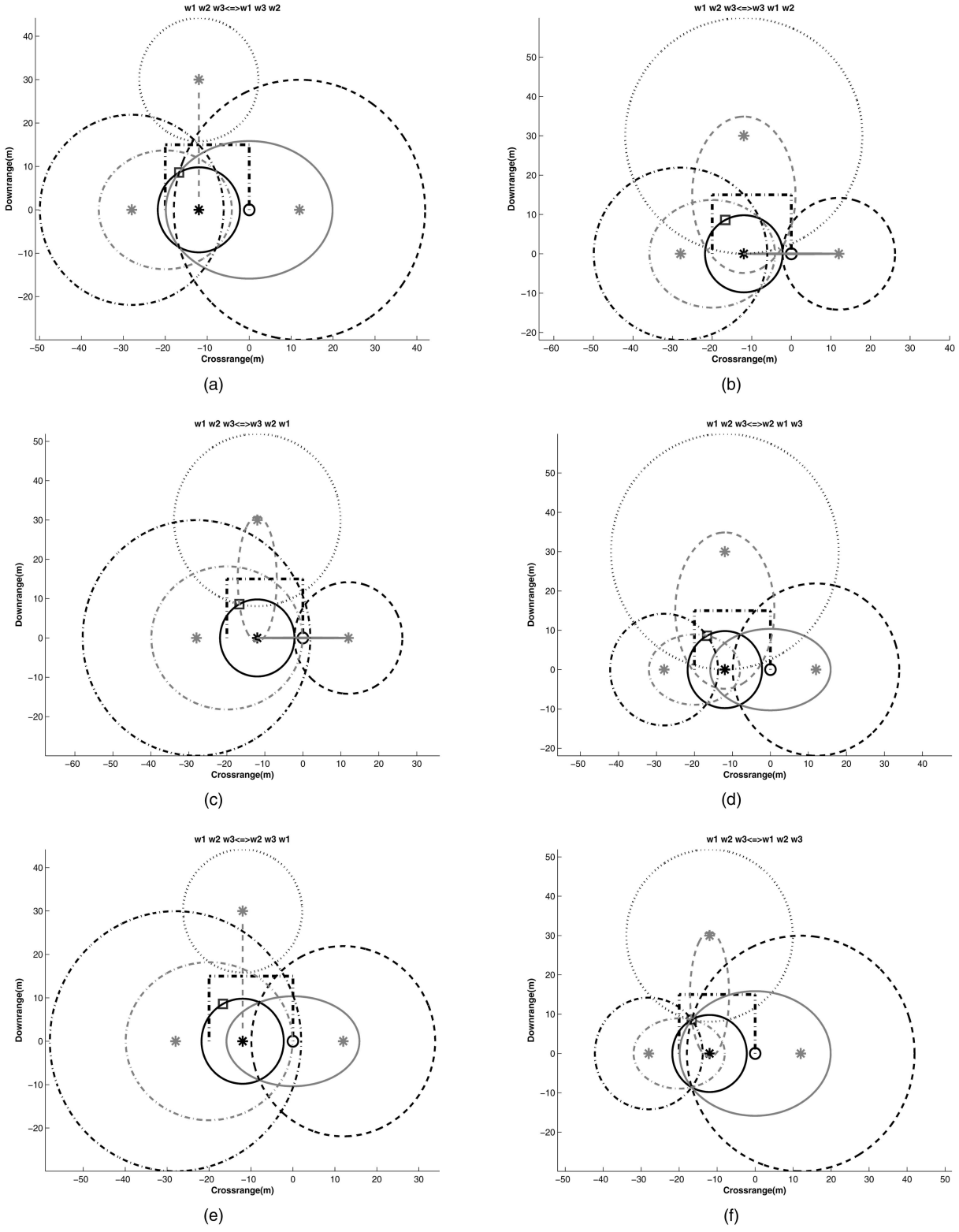

Fig. 5. Wall permutations and associations. (Direct path: black solid line, multipaths w.r.t. wall 1: solid gray and dashed black lines, multipaths w.r.t. wall 2: dashed gray and dotted black lines, multipaths w.r.t. wall 3: gray and black, dashed-dotted lines).

C. Free-Space: Multiple Targets within a Structurce Composed of Oblique Walls

So far, we have considered cases when the walls are perpendicular to one another. The theory as it applies in the paper, may be used when walls are not necessarily at right angles. The slight difference is that the virtual radars will lie on the normals to the walls. The ellipses will then have to be rotated accordingly using Given's rotation matrices. Since the circles are rotation invariant, no additional rotation is required. For example, consider a scene with oblique walls and

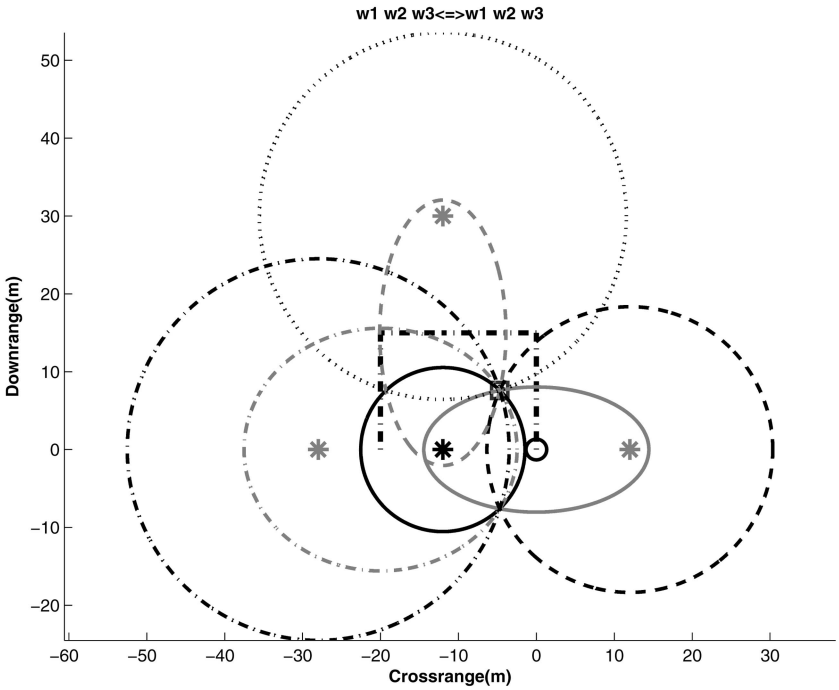

Fig. 6. Example of correct localization after wall associations for single target. (Direct path: black solid line, multipaths w.r.t. wall 1: solid gray and dashed black lines, multipaths w.r.t. wall 2: dashed gray and dotted black lines, multipaths w.r.t. wall 3: gray and black, dashed-dotted lines).

TABLE I
NLS Costs for a Single Target for Associating the TOAs to the Respective Walls

Permutation	1	2	3	4	5	6
NLS Cost in (12) for Fig. 5	1.99e04	1.29e04	2.68e05	1.89e04	5.41e04	0.1227
NLS Cost in (12) for Fig. 6	5.61e02	4.12e03	4.59e03	5.02e03	5.9e03	0.0229

two targets at $\mathbf{x}_t^{(1)} = [-9, 7.5]^T$ and $\mathbf{x}_t^{(2)} = [-4.6, 5.6]^T$. The angle between walls 1 and 2 is 93.4°, while the angle between walls 2 and 3 is 113.6°. The lengths of the walls 1, 2, 3 are 13.45 m, 14.9 m, and 9.2 m, respectively. The rest of the parameters are identical to the scenarios corresponding to Figs. 5 and 6. Consider Fig. 8, which shows the final results after applying the algorithm in Section III. We observe that the virtual radars are located on the normals to the walls, and the ellipses are rotated such that their minor axes are along the respective walls. It is clear from Fig. 8 that the localization is performed correctly. The errors in the NLS estimates are in the second decimal place.

D. Free-Space: Spurious TOAs

We consider the case when spurious TOAs are present in the range profile and are detected. Consider two targets located at $\mathbf{x}_t^{(1)} = [-15.4, 10]^T$, and $\mathbf{x}_t^{(2)} = [-4.6, 5.6]^T$ along with two false TOAs at ranges 11.33 m and 15.21 m. Both false TOAs were chosen such that they are confusable in accordance with (4a), i.e., each lies half-way between the corresponding direct path and first-order multipath of the two targets. We solved this target localization problem using the combinatorial approach, which evaluated the algorithm for all 120 combinations of selecting 14 TOAs out of the set of 16 detected TOAs. The corresponding NLS cost (normalized by the maximum) versus the combinations is shown in Fig. 9. The target coordinates corresponding to the combination corresponding to the minimum NLS cost are the correct estimates, given by $\hat{\mathbf{x}}_t^{(1)} = [-15.40, 9.99]^T$ and $\hat{\mathbf{x}}_t^{(2)} = [-4.67, 5.56]^T$.

E. Through-the-Wall: Multiple targets

For the TTW scene shown in Fig. 4, consider two targets at locations $\mathbf{x}_t^{(1)} = [-15.4, 7.6]^T$ and $\mathbf{x}_t^{(2)} = [-4.6, 14.6]^T$. The parameters D_1 and D_2 are chosen as 20 and 25, respectively, whereas the standoff distance $D_y = 4$. The front wall has a thickness of 0.2 m and dielectric constant of 7.6, and was assumed to be lossless. In order to increase realism, the associated (parallel polarization) reflection and transmission coefficients were incorporated in the simulation to mimic the losses due to reflections and transmission through and at the walls. These reflection and transmission coefficients have standard derivations [22]. The rest of the parameters are identical to

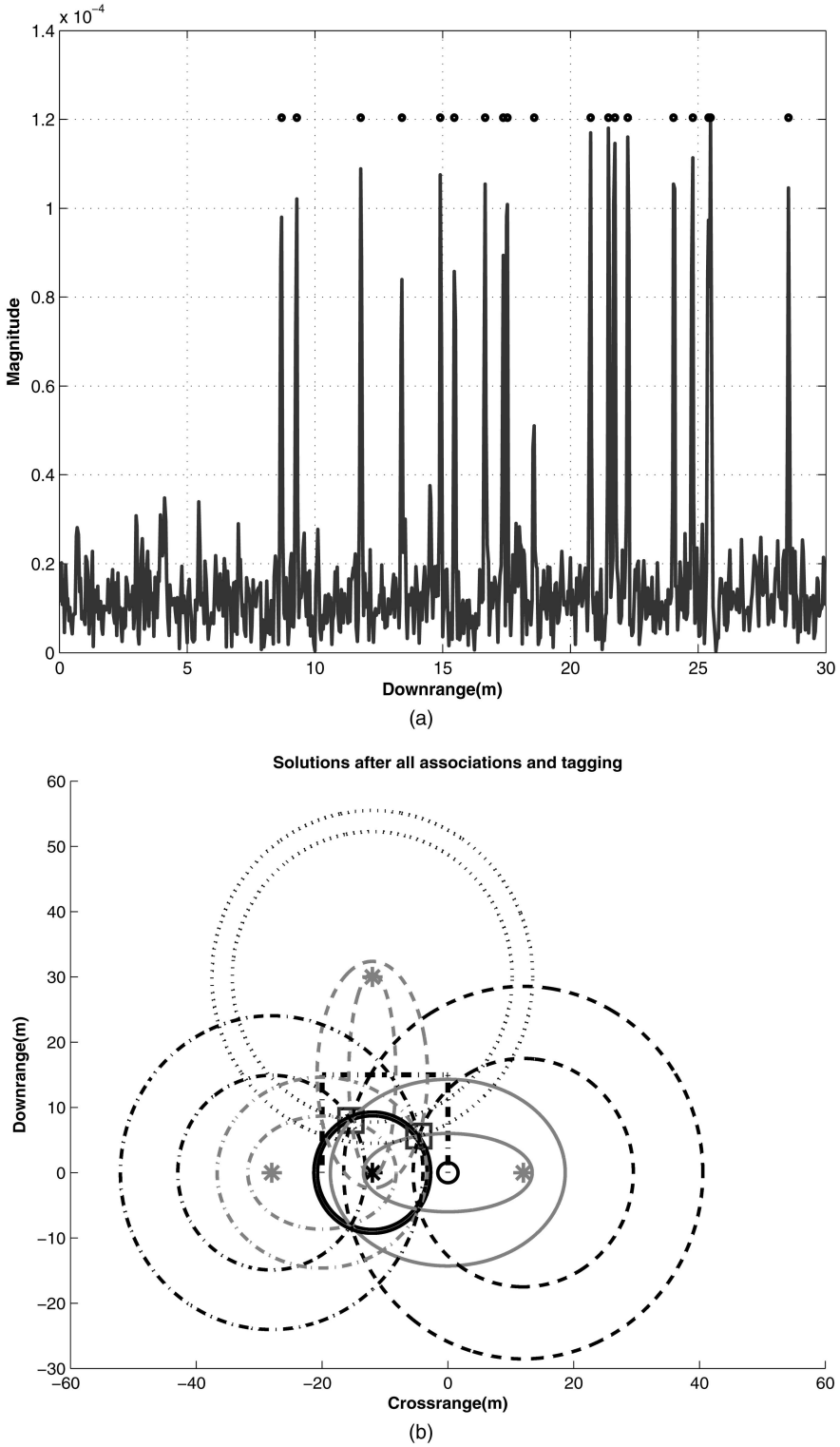

Fig. 7. (a) Correlation peaks (two target case) in 15 dB SNR. (b) Two target localization after clustering and wall associations in 15 dB SNR. (Direct path: black solid line, multipaths w.r.t. wall 1: solid gray and dashed black lines, multipaths w.r.t. wall 2: dashed gray and dotted black lines, multipaths w.r.t. wall 3: gray and black, dashed-dotted lines).

those of the free-space simulation in Fig. 7, no noise was added. The range profile peaks are shown in Fig. 10(a), and as in Fig. 7(a), some of the peaks are again close to each other. Figure 10(b) was obtained by applying the free-space processing of Section II to the TOAs extracted from the range profile. In the figure, we can see that the free-space solution is close to the true solution but does not coincide with it. Specifically, the free-space solution for the first target is given by $[-15.75, 7.37]^T$ and that for the second target is $[-4.30, 14.58]^T$; both have errors in the first decimal place. Note that these free-space

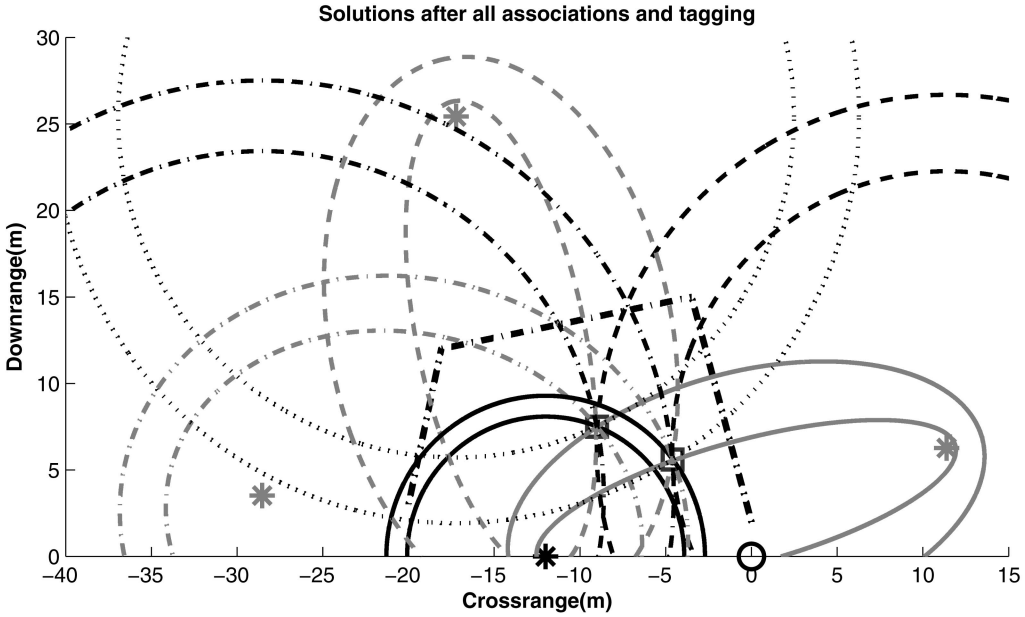

Fig. 8. Scenario where walls are not at right angles, (zoomed in to show detail). (Direct path: black solid line, multipaths w.r.t. wall 1: solid gray and dashed black lines, multipaths w.r.t. wall 2: dashed gray and dotted black lines, multipaths w.r.t. wall 3: gray and black, dashed-dotted lines).

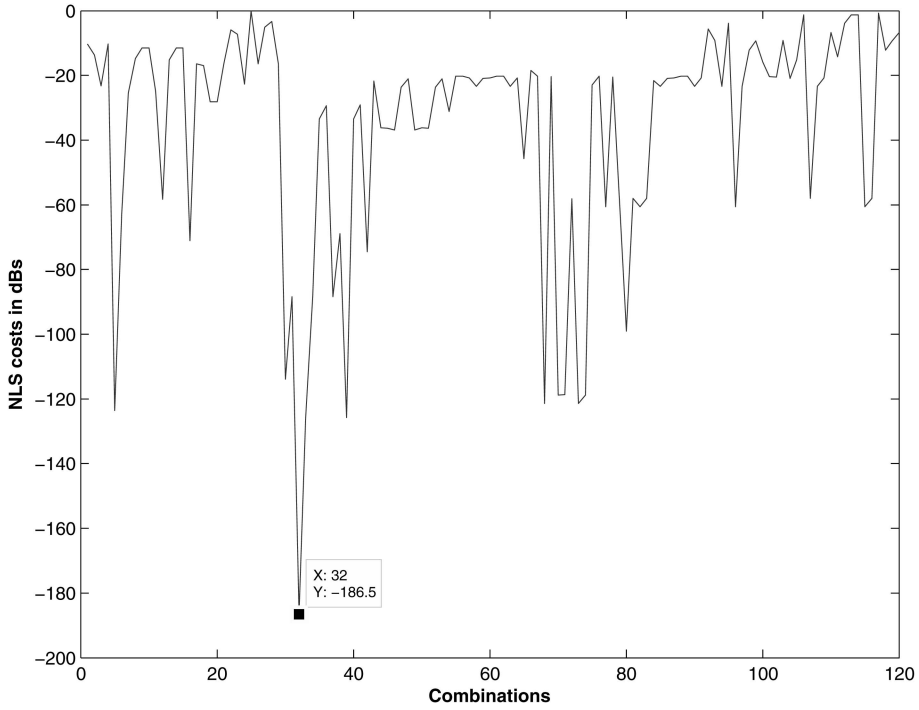

Fig. 9. NLS costs for combinatorial approach to achieve correct localization. Target cordinates at minima are true cordinates.

solutions are obtained from the NLS using (17) for the correct wall association. Continuing the processing to include the TTW specific NLS as described in the algorithm consisting of (18, 19), we obtain the final TTW solutions as $[-15.39, 7.60]^T$ and $[-4.59, 14.61]^T$. The errors are now in the second decimal place.

F. Experimental Results

As a final stage of the investigation, target localization was undertaken using experimental data. The scene shown in Fig. 11 consists of two targets adjacent to a cement board wall. A metal sphere and a dihedral were used as targets and were centered at (0.6 m, 3 m) and (1.9 m, 4.58 m), respectively. The radar coordinates are given by (2.7 m, 0 m). A stepped frequency signal covering the 1–4 GHz frequency band was used. The frequency step-size was chosen to be 15 MHz, giving rise to a maximum unambiguous range of 10 m.

The range profile, obtained after background subtraction and application of frequency domain

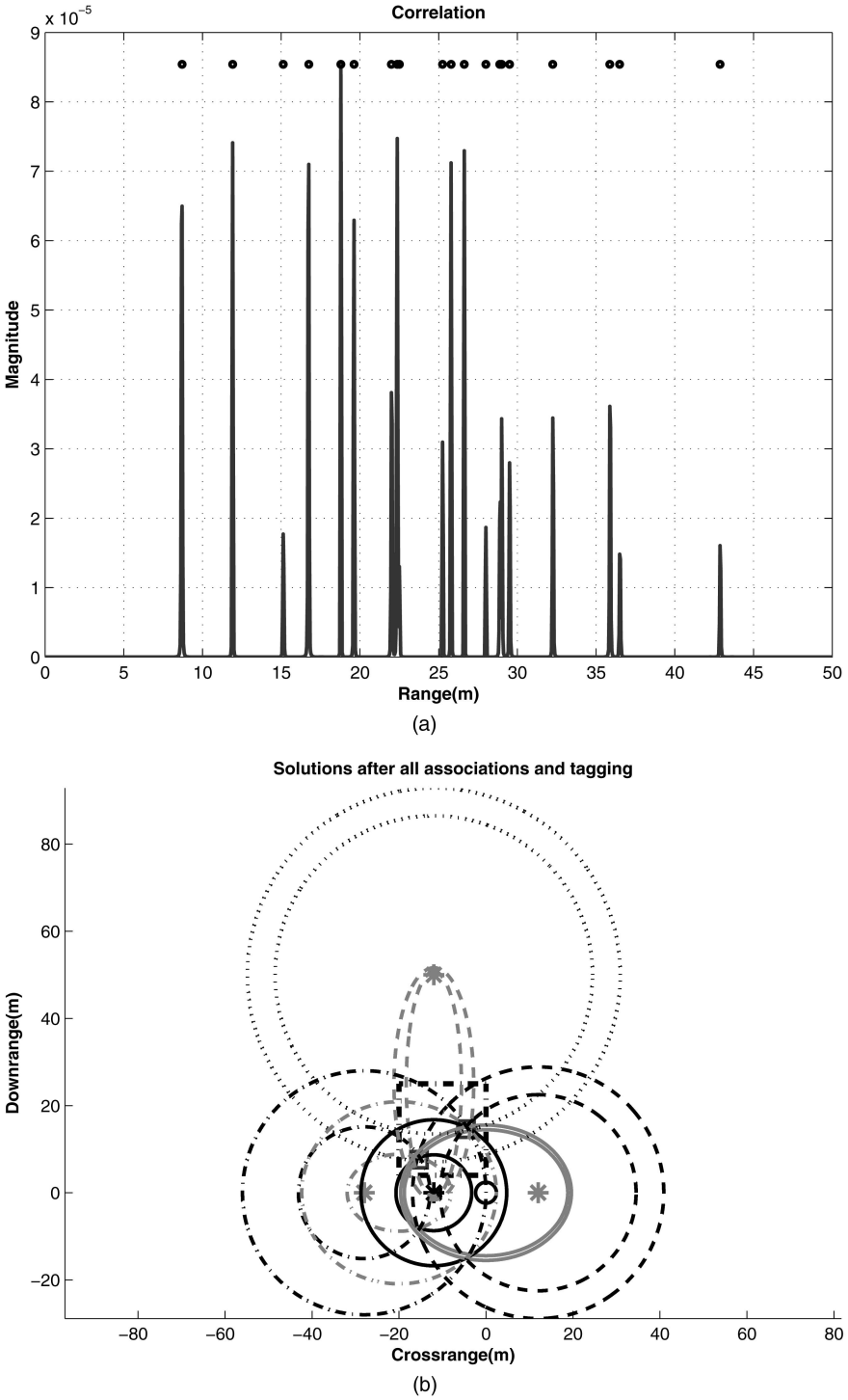

Fig. 10. (a) Correlation peaks (two-target TTW case). (b) Example of a TTW two-target case after using free-space localization. (Direct path: black solid line, multipaths w.r.t. wall 1: solid gray and dashed black lines, multipaths w.r.t. wall 2: dashed gray and dotted black lines, multipaths w.r.t. wall 3: gray and black, dashed-dotted lines).

Kaiser window with parameter set to unity and matched filtering, is shown in Fig. 12(a). As seen in the figure, there exist several peaks between 3 m and 7 m. To increase the accuracy of the estimated target and multipath return TOAs, zero padding was used to interpolate the range profile, and the results are shown in Fig. 12(b). In this figure, the strongest peak is approximately -55 dB; hence, a hard detection threshold of approximately -80 dB was selected, which is -25 dB below the maximum, and is indicated as a dashed-dotted horizontal line in Fig. 12(b). There are now 8 detected peaks, including the creeping wave from the sphere, indicated by an arrow in Fig. 12(b). The creeping wave return occurs $(2+\pi)r$ m after the target return, where r is the radius of the sphere [25]. For the sphere

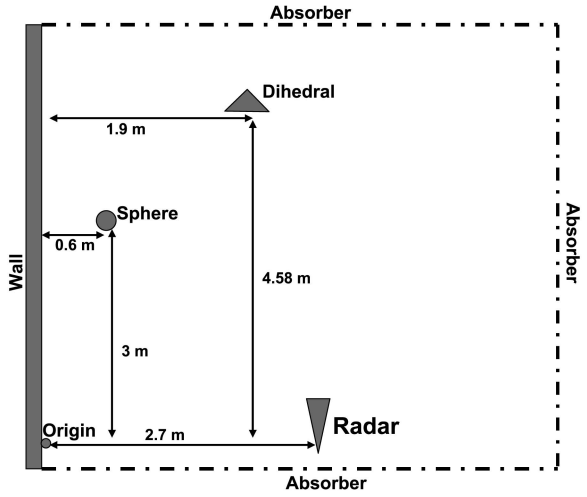

Fig. 11. Experimental setup.

used, the creeping wave return would appear at approximately 4.53 m, which is in agreement with the results in Fig. 12(b). Ideally, we should have six peaks, comprising the direct path and the two multipaths for each target. Ignoring the creeping wave return, we have 7 detected peaks; the spurious peak is attributed to the target-target interaction. The signal SNR varied between 16 dB for the sphere's second-order multipath and 36 dB for the dihedral's direct path.

Since a single wall was used, TOA associations are unnecessary. However, TOA clustering is employed. Ignoring the creeping wave TOA, the target localization results using the combinatorial approach are depicted in Fig. 13. The NLS location estimate for the sphere is (0.544 m, 2.91 m) and for the dihedral is (1.98 m, 4.69 m). The sum of squared error for the sphere and the dihedral is 0.01 m^2 and 0.02 m^2, respectively.

G. Computational Time

For all the simulation and experimental results in this paper, the computational time from clustering and wall associations to the NLS estimation is provided in Table II. These times are based on a workstation with an Intel Xeon 3.72 MHz processor having 4GB memory and running Matlab® version 2007a. The matlab code was not optimized to reduce the computational time. From Table II we find that the computational times for the basic algorithm is less than 2 s. This amounts to target locations being updated 30 times per minute, which is appropriate for slow-moving persons inside buildings. For stationary targets, computational time is not an issue.

VI. CONCLUSIONS

In this paper we have demonstrated that by utilizing the multipath reflections, target localization may be achieved with a single sensor. We showed that by exploiting the multipath returns arising from a single wall to create an additional virtual sensor, the target could be considered part of a monostatic and a bistatic geometry. When the two geometries apply, an analytical solution for the target location was obtained. To localize a target correctly in the

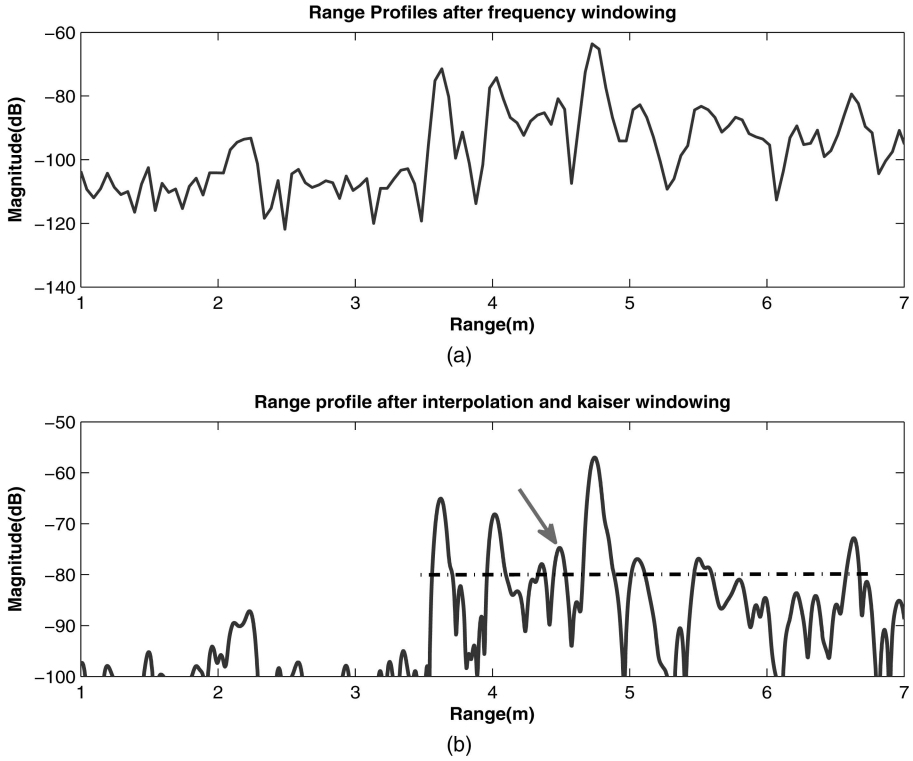

Fig. 12. Range profiles of expeiment. (a) After using kaiser window. (b) After interpolation and windowing.

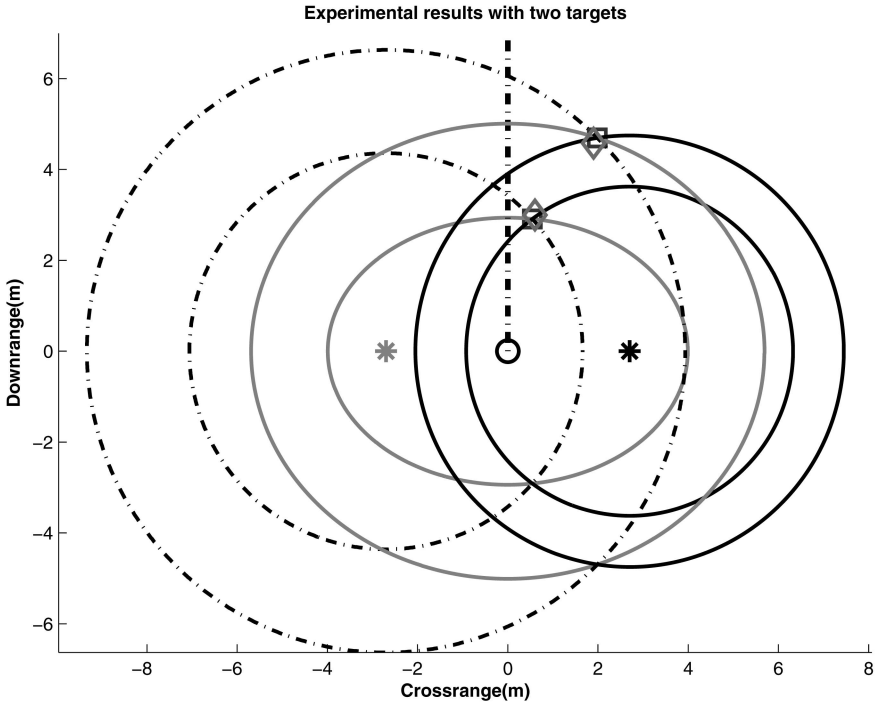

Fig. 13. Noncoherent localization results for experiment, estimated NLS (□) and true (◇) solutions are shown. Direct path cricles (black solid lines), ellipses (gray solid lines), and monostatic circles centerted at VR (black dashed-dotted) intersect in region close to true solutions.

TABLE II
Matlab® Computational Time from Clustering to Final NLS Localization

Figure Number	5	6	7(b)	8	9	10	13
Computational Time	0.65 s	0.67 s	1.19 s	1.31 s	65 s	1.4 s	1.9 s

presence of multiple walls, as may arise in a TTW or in an urban canyon situation, the multipath TOAs must be correctly associated to their respective walls. An algorithm to perform such an association was devised. Furthermore, it was shown that in the case of multiple targets, localization is achievable provided the multipaths and direct paths are all resolved.

Extension of these noncoherent localization techniques to TTW radar was demonstrated. An NLS approach was developed which provides correct location estimates by allowing for the change in propagation velocity and the refraction that occur as the wave interacts with the front wall. Simulation and experimental results were presented which validated the proposed techniques.

REFERENCES

[1] Baranoski, E. J.
Through-wall imaging: Historical perspectives and future directions.
Journal of the Franklin Institute, **345**, 6 (Sept. 2008), 556–569.

[2] Frazier, L. M.
Surveillance through walls and other opaque materials.
IEEE Aerospace and Electronic Systems Magazine, **11**, 10 (Oct. 1996), 6–9.

[3] Ferris, Jr., D. D. and Currie, N. C.
A survey of current technologies for through-the-wall surveillance (TWS).
In *Proceedings of the SPIE Conference C3I Information, and Training Technologies for Law Enforcement*, vol. 3577, Boston, MA, Jan. 1999, pp. 62–72.

[4] Greneker, III, E. F.
RADAR flashlight for through-the-wall detection of humans.
In *Proceedings of the SPIE Conference on Targets & Backgrounds: Characterization & Representation IV*, vol. 3577, July 1998, pp. 280–285.

[5] Amin, M. G. (Ed.)
Through-the-Wall Radar Imaging.
Boca Raton, FL: CRC Press, Dec. 2010.

[6] Dogaru, T. and Le, C.
SAR images of rooms and buildings based on FDTD computer models.
IEEE Transactions on Geoscience and Remote Sensing, **47**, 5 (2008), 1388–1401.

[7] Yoon, Y-S. and Amin, M.
Spatial filtering for wall-clutter mitigation in through-the-wall radar imaging.
IEEE Transactions on Geoscience and Remote Sensing, **47**, 9 (Aug. 2009), 3192–3208.

[8] Ahmad, F., Amin, M., and Kassam, S. A.
Synthetic aperture beamformer for imaging through a dielectric wall.
IEEE Transactions on Aerospace and Electronic Systems, **41**, 1 (Jan. 2005), 271–283.

[9] Ahmad, F., Zhang, Y., and Amin, M.
Three-dimensional wideband beamforming for imaging through a single wall.
IEEE Geoscience and Remote Sensing Letters, **5**, 2 (Apr. 2008), 176–179.

[10] Wang, G., Amin, M., and Zhang, Y.
A new approach for target locations in the presence of wall ambiguity.
IEEE Transactions on Aerospace and Electronic Systems, **42**, 1 (Jan. 2006), 301–315.

[11] Martone, A., Ranney, K., and Innocenti, R.
Automatic through the wall detection of moving targets using low-frequency ultra-wideband radar.
In *Proceedings of the IEEE International Radar Conference*, Washington, D.C., 2010.

[12] Ahmad, F. and Amin, M.
Noncoherent approach to through-the-wall radar localization.
IEEE Transactions on Aerospace and Electronic Systems, **42**, 4 (Oct. 2006), 271–283.

[13] Ahmad, F., Amin, M., and Zemany, P. D.
Dual frequency radars for target localization in urban sensing.
IEEE Transactions on Aerospace and Electronic Systems, **45**, 4 (Oct. 2009), 1598–1609.

[14] Burkholder, R. J.
Electromagnetic models for exploiting multi-path propagation in throughwall radar imaging.
In *Proceedings of the International Conference on Electromagnetics in Advanced Applications*, Torino, Italy, Sept. 2008, pp. 572–575.

[15] Linnehan, R. and Schindler, J.
Multistatic scattering from moving targets in multipath environments.
In *Proceedings of the IEEE International Radar Conference*, Pasadena, CA, May 4–8, 2009.

[16] Sen, S., Hurtado, M., and Nehorai, A.
Adaptive OFDM radar for detecting a moving target in urban scenarios.
In *Proceedings of the International Waveform Diversity and Design Conference*, Orlando, FL, Feb. 8–13, 2009.

[17] Krolik, J. L., Farell, J., and Steinhardt, A.
Exploiting multipath propagation for GMTI in urban environments.
In *Proceedings of the IEEE Radar Conference*, Verona, NY, Apr. 24–27, 2006.

[18] Deiana, D., Kossen, A. S., and van Rossum, W. L.
Multipath exploitation in an urban environment using a MIMO surveillance radar.
In *Proceedings of the International Radar Conference*, Vilnius, Lithuania, June 16–18, 2010.

[19] Chakraborty, B., et al.
Multipath exploitation with adaptive waveform design for tracking in urban terrain.
In *Proceedings of the IEEE International Conference on Acoustics, Speech, and Signal Processing*, Dallas, TX, Mar. 14–19, 2010.

[20] Setlur, P.
Statistical algorithms and bounds for moving targets in urban sensing and through-the-wall radar applications.
Ph.D. thesis, Villanova University, May 2010.

[21] Liu, K. W. K. and So, H. C.
Range-based source localisation with pure reflector in presence of multipath propagation.
Electronics Letters, **46**, 13 (June 2010), 957–958.

[22] Balanis, C. A.
Advanced Engineering Electromagnetics.
Hoboken, NJ: Wiley, Apr. 2009.

[23] Li, X. and Pahlavan, K.
Super-resolution ToA estimation with diversity for indoor geolocation.
IEEE Transactions on Wireless Communications, **3**, 1 (Jan. 2004), 224–234.

[24] Do, J., Rabinowitz, M., and Enge, P.
Linear time-of-arrival estimation in a multipath environment by inverse correlation method.
In *Proceedings of the Institute of Navigation*, Cambridge, MA, June 27–29, 2005.

[25] Ahmad, F., et al.
Design and implementation of nearfield, wideband synthetic aperture beamformers.
IEEE Transactions on Aerospace and Electronic Systems, **40**, 1 (Jan. 2004), 206–220.

Pawan Setlur was born in Bangalore, India. He has a bachelor's degree in electrical and electronics engineering from India, and obtained his Ph.D. in electrical engineering in May 2010 from Villanova University.

His Ph.D. research focused on moving targets in through-the-wall radar and urban sensing. His research interests are in the general areas of signal processing, radar, and statistics.

Graeme E. Smith (M'08—SM'10) obtained his Ph.D. from University College London in 2008, M.Sc. in information systems from Robert Gordon University in 1999, and B.Sc. in physics from University of Southhampton in 1998.

He has over ten years experience in radar engineering working first in industry before turning to academic research in 2004. His current research interests are focused on the classification of stationary targets in through-the-wall radar images, a field that combines radar signal processing, classification, and electromagnetic phenomenology. Before joining the Center for Advanced Communications at Villanova he was a post doctoral fellow at University College London (UCL). There his research interests included the development of passive bistatic radar systems using 802.11 WiFi signals for indoor surveillance and 802.16 WiMAX transmissions for maritime surveillance. At UCL his interests also included the use of the micro-Doppler signature for target recognition in battlefield radar. Prior to joining UCL he worked as a systems engineer for BAE SYSTEMS for five years on projects relating to the radar warning receivers of the EuroFighter, Harrier and UK Attack Helicopter.

Dr. Smith is author to over fifteen conference and journal papers and one book chapter. He is a member of the IET.

Fauzia Ahmad (S'97—M'97—SM'06) received her MS degree in electrical engineering in 1996, and Ph.D. degree in electrical engineering in 1997, both from the University of Pennsylvania, Philadelphia, PA.

From 1998 to 2000, she was an assistant professor in the College of Electrical and Mechanical Engineering, National University of Sciences and Technology, Pakistan. During 2000–2001, she served as an assistant professor at Fizaia College of Information Technology, Pakistan. Since 2002, she has been with the Center for Advanced Communications, Villanova University, Villanova, PA, where she is now a research associate professor and the director of the Radar Imaging Lab.

Dr. Ahmad has over 85 journal and conference publications in the areas of radar imaging, array signal processing, sensor networks, compressive sensing, and over-the-horizon radar.

Moeness Amin (M'83—SM'91—F'01) received his Ph.D. degree in 1984 from the University of Colorado, in electrical engineering. He has been on the Faculty of the Department of Electrical and Computer Engineering at Villanova University since 1985. In 2002, he became the Director of the Center for Advanced Communications, College of Engineering.

He is the recipient of the 2009 Individual Technical Achievement Award from the European Association of Signal Processing, and the recipient of the 2010 NATO ScientificAchievement Award. He is a Fellow of the International Society of Optical Engineering and a Fellow of the Institute of Engineering and Technology (IET). Dr. Amin is a recipient of the IEEE Third Millennium Medal; recipient of the Chief of Naval Research Challenge Award, 2010; Distinguished Lecturer of the IEEE Signal Processing Society, 2003–2004; Active Member of the Franklin Institute Committee on Science and the Arts; recipient of Villanova University Outstanding Faculty Research Award, 1997; and the recipient of the IEEE Philadelphia Section Award, 1997. He is a member of IEEE, SPIE, EURASIP, ION, Eta Kappa Nu, Sigma Xi, and Phi Kappa Phi.

He has over 450 journal and conference publications in the areas of wireless communications, time-frequency analysis, smart antennas, waveform design and diversity, interference cancellation in broadband communication platforms, anti-jam GPS, target localization and tracking, direction finding, channel diversity and equalization, ultrasound imaging and radar signal processing. He is a recipient of seven best paper awards. Dr. Amin currently serves on the Overview Board of the *IEEE Transactions on Signal Processing*. He also serves on the Editorial Board of the *EURASIP Signal Processing Journal*. He was a plenary speaker at ICASSP 2010. Dr. Amin was the Special Session Cochair of the 2008 IEEE International Conference on Acoustics, Speech, and Signal Processing.

He was the Technical Program Chair of the 2nd IEEE International Symposium on Signal Processing and Information Technology, 2002. Dr. Amin was the General and Organization Chair of the IEEE Workshop on Statistical Signal and Array Processing, 2000. He was the General and Organization Chair of the IEEE International Symposium on Time-Frequency and Time-Scale Analysis, 1994. He was an Associate Editor of *IEEE Transactions on Signal Processing* during 1996–1998. He was a member of the IEEE Signal Processing Society Technical Committee on Signal Processing for Communications during 1998–2002. He was a member of the IEEE Signal Processing Society Technical Committee on Statistical Signal and Array Processing during 1995–1997.

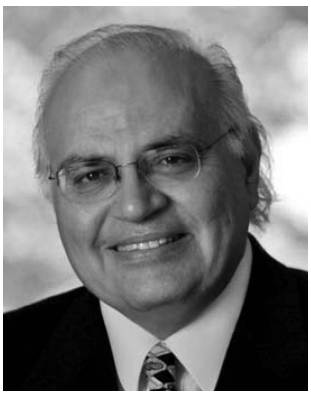

Dr. Amin was the Guest Editor of the *Journal of Franklin Institute*, *Special Issue on Advances in Indoor Radar Imaging*, September 2008. He was a Guest Editor of the *IEEE Transactions on Geoscience and Remote Sensing*, *Special Issue on Remote Sensing of Building Interior*, May 2009, and a Guest Editor of the *IET Signal Processing*, *Special Issue on Time-Frequency Approach to Radar Detection, Imaging, and Classification*, December 2009.